



Eccentricity Effect on Radial Forces of Bearingless BLDC Motor: Study and Analysis

Ali A. Yousif ^{a*}, Ahmed M. Mohammed ^b, Mohammed Moanes E. Ali ^c

^a Electrical Engineering Dept., University of Technology-Iraq, Alsina'a Street, 10066 Baghdad, Iraq.

*Corresponding author Email: cee.19.10@grad.uotechnology.edu.iq

HIGHLIGHTS

- The magnetostatic analysis is used to evaluate the effect of the permanent magnet.
- The transient analysis evaluates the effect of both the magnet and the armature current.
- The lowest value of the radial force exists when the rotor is at the center position.
- The radial force increases directly with the rotor displacement.
- The radial force is variable because the air gap reluctance varies with rotor angle.

ABSTRACT

The bearingless BLDC motor gathers all advantages of the BLDC motor and bearingless machine, and this motor is extensively used in blood and artificial heart pumps. In a bearingless BLDC motor, there are two sets of windings, the main winding, responsible for producing the motor torque, and the suspension winding, which keeps the rotor in the center without any contact with the stator. Generally, the suspension system is responsible for the generation of the suspension forces to cancel the pull-out forces (radial forces), which strongly depends on the accurate evaluation of radial forces distribution at different operating conditions. In this paper, a mathematical model based on the finite element method is used to calculate and analyze the radial force of a bearingless blood pump BLDC motor using Ansys/Maxwell. Based on Maxwell equations, the normal and tangential components of the airgap flux density is determined and used to calculate the radial force, magnitude, and direction. In addition, different cases of rotor displacement under eccentricity conditions are covered. The relation between the rotor displacement and radial force is analyzed, accounting for the displacement direction. Finally, the results are analyzed and discussed.

ARTICLE INFO

Handling editor: Ivan A. Hashim

Keywords:

Bearingless; Eccentricity; BLDC; Radial Force; Finite element method; Ansys/Maxwell

1. Introduction

A Brushless Direct Current (BLDC) motor is defined as an electronically switched, self-synchronous rotary motor where the stator contains three-phase armature winding. The rotor includes permanent magnets with rotor-position sensors. This motor has many advantages: simple design, high performance, high torque, no spark, no noise, and long operating life [1,2].

Usually, the shaft of the BLDC motor is supported by two bearings. Many motoring applications need special requirements such as reliability, high purity, or/and high speed. The magnetic bearing motor has been used in such an application because of the benefits of no contact, no lubrication, and no maintenance. However, conventional magnetic bearings occupy a large space and are usually expensive, limiting the magnetic bearings technique in wide industry applications [2]. In such a case, the alternative is the bearing less machine, which has the suspension and torque windings. These windings are wound together in the stator slots so that the airgap flux density distribution is unbalanced by adding the suspension flux to the main motor flux. As a result, the rotor shaft is stably rotated and suspended without mechanical contact [3]. The bearingless BLDC motor, with all advantages of the BLDC motor and bearing less machine, has a wide application prospect from biomedicine to aerospace. Compared with the pure magnetic bearing, bearing less BLDC motor overcomes its shortages of axial space length, the motor of large volume, complex system structure, and expensive [4]. Bearingless BLDC motor is extensively used in artificial heart pumps, Because of its many important advantages, such as its low weight and small size, it is distinguished as a very high-speed motor, there is no heat generation, and there is no material wear, it is magnetically levitated and has no mechanical contact, and has zero friction, it has less probability of failure [5].

The design of the suspension system depends significantly on the accurate evaluation of the radial force and determines the factor that affects it. The radial force is applied on the rotor in a radial direction toward the center or away. It plays an important role in the radial locating of the rotor inside the motor bore. For bearingless motors, tangential and radial forces are generated under permanent magnets and the armature currents. Depending on the radial force of the suspension winding, the radial forces can be calibrated in such a way as to cancel each other to satisfy the bearing less operation [6].

In this paper, the finite element method has been implemented to calculate the radial force of the bearingless BLDC motor by using Ansys/Maxwell 16 software. The radial force is affected by many factors, such as the rotor's stator current, radial position, and rotation angle. The effect of these factors has been studied at different working conditions.

The most recent studies on the third generation of blood pumps use a bearing less instead of a mechanical bearing. Yuemei [4] introduces a multi-phase, double-stator bearing less BLDC motor, and the author proposed a mathematical model of the levitation forces. The optimizations are carried out to minimize the cogging torque and improve the motor performance. Xiaowan [7] introduces a mathematical model of the suspension force drive, using the equivalent magnetic circuit method to establish the electromagnetic relationship inside the motor and the virtual displacement method. Using the finite element analysis method, the study analyzed the change of the suspension force amplitude under different currents and the influence of different eccentric displacements on the unbalanced magnetic tension.

Thus, this paper aims to show the effect of the radial force on the performance of BLDC machines by taking the cases of deviation of the rotor from the center and making mathematical and numerical calculations for the radial force. This paper mainly focuses on studying and analyzing the radial force using magnetostatic and transient solvers bearing less BLDC motor for blood pump application. The article is organized as follows: Section 2 introduces the principle of radial force generation. Section 3 presents the mathematical model and theoretical equations of the radial force. Section 4 illustrates the results, and section 5 provides the conclusion.

2. Principle of Radial Force Generation

Figure 1 depicts the principles of radial force generation in bearingless motors. The rotor and stator are magnetized with four poles. There are strong magnetic attractive forces between the rotor and stator center's position under these magnetic poles. These four poles have the same flux density and, as a result, have the same attractive force magnitudes (see Figure 1a). Figure 1b shows the unbalanced condition since one north pole is greater than the other. As a result, the attractive force is stronger as the rotor moves in the direction of the force, and it is inherently unstable. Under this condition, the rotor is subjected to a radial magnetic force due to unbalanced airgap flux density distribution [8]. In numerical methods, Maxwell's stress tensor is commonly used to calculate the forces and torques. The concept is based on Faraday's statement that stress develops in flux lines. Figure 2 shows the airgap flux density solution, tangential and radial (normal) components, and field strength. This figure shows that the flux lines cross the air gap tangentially, causing a significant rotating torque to move the rotor counterclockwise. The magnetic field intensity between objects in a vacuum, according to Maxwell's stress theory, causes a stress force σ_F on the object surfaces, which is given by

$$\sigma_F = \frac{1}{2} \mu_0 \cdot H^2 = \frac{B^2}{2\mu_0} \quad (1)$$

$$B = \mu_0 \cdot H \quad (2)$$

Where B is flux density, H is the field strength and μ_0 is the permeability of free space. The stress is produced perpendicular to the lines of force and in the direction of the force. The stress can be divided to; it's normal (σ_{Fn}) and tangential (σ_{Ftan}) components, σ_{Ftan} contributes to electromagnetic torque, whereas σ_{Fn} causes unbalanced rotor vibration and, consequently, acoustic sounds. With the object in concern [6, 9], we get:

$$\sigma_{Fn} = \frac{1}{2} \mu_0 \cdot (H_n^2 - H_{tan}^2) \quad (3)$$

$$\sigma_{Ftan} = \mu_0 \cdot H_n \cdot H_{tan} = \mu_0 \cdot H_n \cdot A = B_n \cdot A \quad (4)$$

3. Calculation of Radial Force

3.1 The Stress Tensor Method

The Tension between the magnetic field of the permanent magnet and the MMF of the stator is the radial force density, usually referred to as the radial strain. To measure this electromagnetic force acting on an object, the stress tensor method of Maxwell is commonly used for producing magnetic stresses, forces, and torque in electrical machines. In 2-D finite element analysis (FEA), the radial and tangential components of the force are measured. Such forces are given as:

$$F_{rad(\Phi_r)} = \frac{1}{2\mu_0} [B_r^2 - B_t^2] \quad (5)$$

$$B_t = B_{tPM} + B_{tS} \quad (6)$$

$$B_r = B_{rPM} + B_{rS} \quad (7)$$

Where B_{rPM} , B_{tPM} , B_{rS} and B_{tS} Represent the radial and tangential flux densities produced by the magnet and stator winding in tesla, respectively. For bearingless BLDC motor, both B_r and B_t They are created by two sources, the winding current, and the PMs. If no excitation current (i.e., the stator current is zero), the flux density components are produced by PMs only. The values B_{rPM} , B_{rS} , B_{tPM} , and B_{tS} can be expressed theoretically by Fourier series as:

$$B_{tPM} = \sum_{K=1}^{\infty} B_{tPMK} \sin(K\varphi_r) \tag{8}$$

$$B_{tS} = \sum_{K=1}^L B_{tSK} = B_{t-as} + B_{t-bs} + B_{t-cs} \tag{9}$$

$$B_{rPM} = \sum_{K=1}^{\infty} B_{rPMK} \cos(K\varphi_r) \tag{10}$$

$$B_{rS} = \sum_{K=1}^L B_{rsk} = B_{r-as} + B_{r-bs} + B_{r-cs} \tag{11}$$

The tangential and radial components of the flux contributed by one phase current can be expressed in the form as:

$$B_{t-as}(\varphi_S) = i_{aS} B_1(\varphi_S) \tag{12}$$

where, $B_1(\varphi_S)$ is an even (zero average) periodic function concerning φ_S . φ_S and φ_r are the stator and rotor position angles, respectively.

$$B_{r-as}(\varphi_S) = i_{aS} B_2(\varphi_S) \tag{13}$$

where, $B_2(\varphi_S)$ is a zero average odd periodic function concerning φ_S . The phase (A) current is:

$$i_{aS} = i_S \cos(\theta_r + \varphi_i) \tag{14}$$

Equations (12, 13, and 14) can be applied similarly for phases b and c with a current phase shift of 120° and 240°, respectively. Electrical angles φ_S , φ_r and θ_r Are defined by multiplying the mechanical angles by the number of pole pairs.

$$\varphi_S = \varphi_r + \theta_r \tag{15}$$

Once the distribution of the air gap flux is known, it is possible to measure the radial force per unit area at any point of the air gap according to [10, 11]:

$$F_{rad} = \frac{P}{2} \int_0^{2\pi} F_{rad}(\varphi_r) \cdot R \cdot l \cdot d\varphi_r \tag{16}$$

R represents the radius of the contour in mm, l is the stack length of the machine core in mm, and P is the number of poles.

3.2 The Radial Force Under Rotor Eccentricity

When the rotor is in the normal center, the air gap length between the rotor and stator is defined as g_0 . However, if the rotor center moves toward the x or/and y-axis, the air gap length will be changed and defined as $g(\phi)$, as shown in Figure 3. Equation 17 determines the value of air gap length under eccentricity conditions at any x and y displacement where (ϕ) is the spatial mechanical angle, and the inverse of air gap length is shown in Equation 18 when the removal is small compared to (g_0) [8].

$$g(\phi) = g_0 - x \cos(\phi) - y \sin(\phi) \tag{17}$$

$$\frac{1}{g(\phi)} = \frac{1}{g_0} \left(1 + \frac{x}{g_0} \cos(\phi) + \frac{y}{g_0} \sin(\phi) \right) \tag{18}$$

Figure 4 shows the direction of the resultant radial force and flux direction when the rotor was under eccentricity condition ($\phi=0$) and displacement distance (x) toward the x-axis direction. It can be seen that an unbalanced radial force will be generated in the air gaps 1, 2, 3, and 4. The rotor has an eccentric displacement in the air gaps 1, which produces an attractive force in this direction [12].

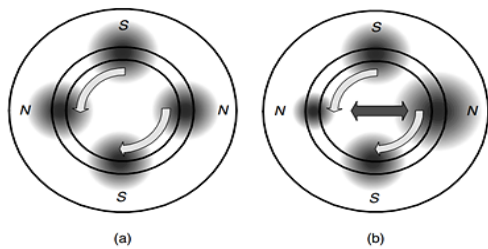


Figure 1: Radial force in the air gap at (a) Balanced flux density, (b) Unbalanced flux density

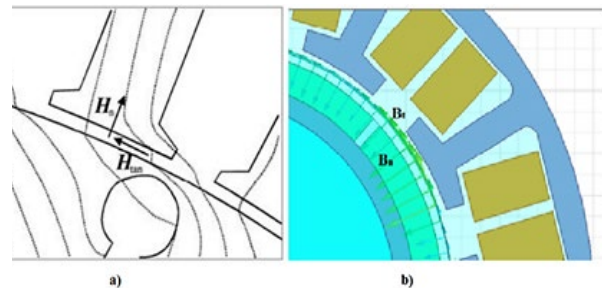


Figure 2: Radial and tangential components of (a) the field strength, (b) flux density vectors

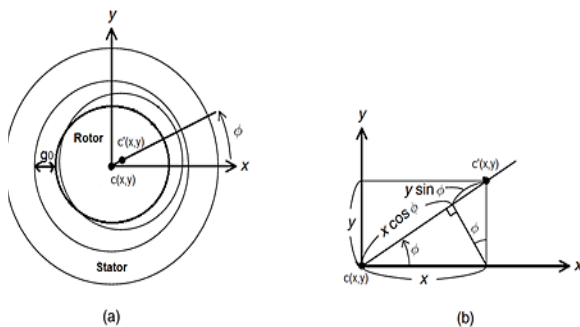


Figure 3: Variation of air gap length with rotor displacement: (a) variation rotor enters, and (b) coordinate description [8]

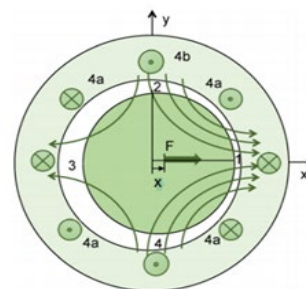


Figure 4: Radial force distribution with a deviation of the rotor from the center

3.3 Machine Topology and Radial Force Relation

The radial force distribution is also influenced by the slot/pole combination of the machine. For 12 slots/ 8 pole machines, the least common multiple (LCM) is (24), and the number is symmetric, which corresponds to the greatest common divisor is (4). This number of symmetric slot/pole configurations makes the machine work under balanced flux density distribution and minimize radial force effect. As it can be seen, the three-phase winding connection sequence is (A-A'-B-B'-C-C') where A', B', C' is the return phases corresponding to phases A, B, C, respectively, as shown in Figure 5(a) [13, 14]. According to the number of symmetries, the 12/8 machine can be divided into four symmetric parts. Therefore, one of four machine parts has been modeled with odd boundary conditions using FEM, as shown in Figure 5(b).

4. Analysis and Results

4.1 BLDC Machine Model

In this work, blood pump bearingless BLDC motor application has been selected as a case of study to investigate the effect of rotor displacement on radial force and machine performance. The parameters of the studied motor are listed in Table 1. Figure 6 shows the 2-D FE model with a flux density plot. The motor is analyzed under underrated working conditions [15].

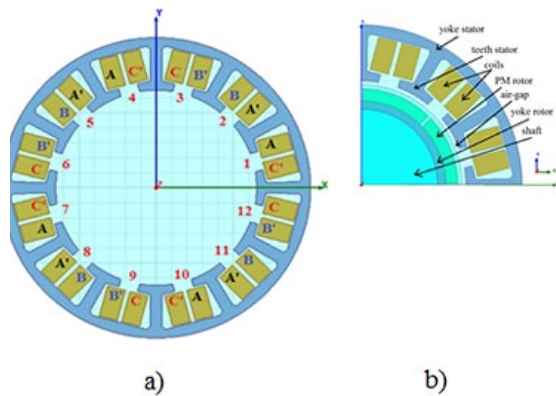


Figure 5: Geometry and winding configuration of the BLDC motor: (a) complete model, (b) one quarter model

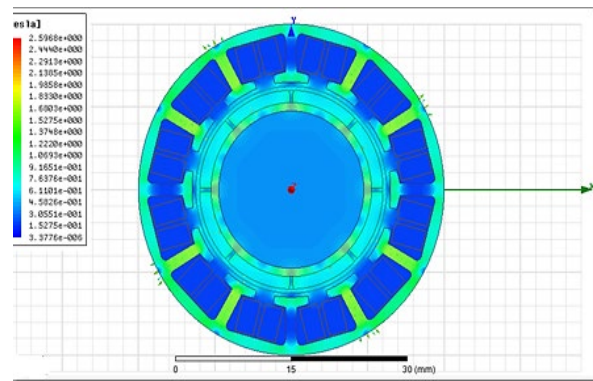


Figure 6: Cross-sectional view of the bearingless BLDC motor

Table 1: Specification of blood pump bearingless BLDC motor

Parameters	Value	Parameters	value
No. of phase	3	Slot body height	4mm
No. of conductor/slot	32	Slot wedge max. width	6mm
No. of winding layers	2	Slot body bottom width	8mm
Stack length	10mm	Slot body bottom fillet	0.6mm
No. of stator slot	12	No. of rotor Poles	8
Stator outer diameter	40mm	Rotor outer diameter	24mm
Stator inner diameter	26mm	Rotor Inner Diameter	19mm
Slot opening height	1mm	Magnet span ratio	0.95
Slot opening width	2.5mm	Magnet thickness	1.5mm

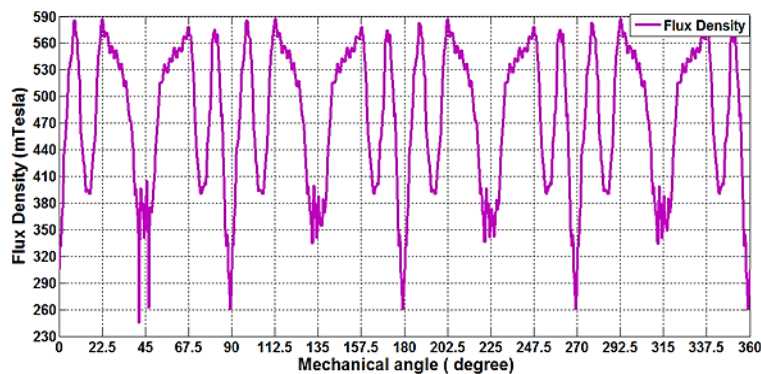


Figure 7: Flux density distribution in the air gap when the rotor is at the center position

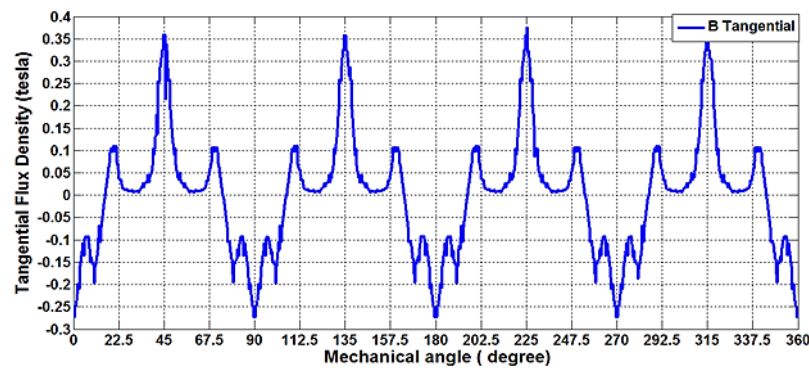


Figure 8: Tangential flux density

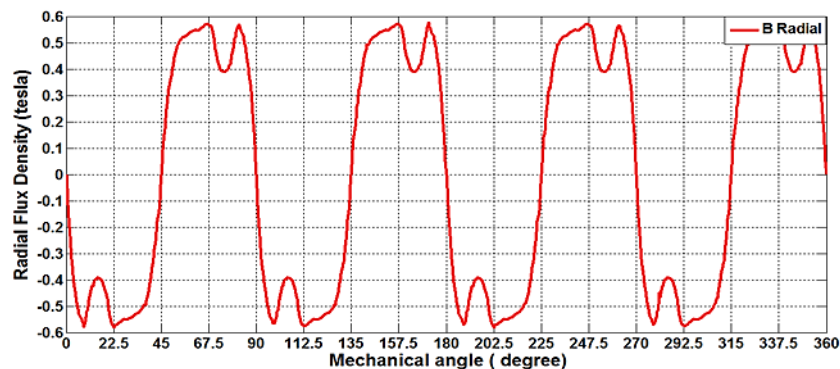


Figure 9: Radial (normal) flux density

4.2 Results and Discussion

From the magnetostatic solver, Figure 7 shows flux density distribution generated by the permanent magnet only. The flux is balanced in the air gap over one complete mechanical revolution without rotor eccentricity. When the rotor is at the center position, the tangential and radial flux densities in the air gap are shown in Figure 8 and Figure 9, respectively.

When the rotor moves toward the x-axis direction, the air gap flux density is not uniform. Figure 10 shows the radial and tangential flux density in the air gap. The permanent magnet generates the largest flux density when the rotor moves from the stator center in the x-axis direction by 0.45 mm (maximum allowable displacement). When the rotor moves toward the y-axis direction, the air gap flux density is distorted, and the largest magnitude can be found when the air gap length is minimum. Figure 11 shows the radial and tangential flux density at eccentricity conditions. It can be seen that the value of the flux density is higher in the upside of the air gap, the largest flux density generated by the permanent magnet when the rotor moves from the stator center in the y-axis direction by 0.45 mm.

Both B_r and B_t They are produced from the stator current and the PM. But, since the machine is in the static condition, the current is considered zero. Since the BLDC machine usually has a relatively large air gap, this study ignored the saturation. The radial force distribution is calculated over (360°) mechanical degree as shown in Figure 12 (a). The resultant radial force is obtained by using the static state solver. When the rotor rotates at the center (no eccentricity), the resultant radial force over one rotor revolution is shown in Figure 12 (b). The results obtained using the Maxwell stress tensor equations show that the radial force distribution is symmetrical when the stator current is zero and the rotor is at the center.

When the rotor is eccentricity by 0.1 mm, 0.25 mm, and 0.45 mm in y-direction, the radial force distribution is shown in Figure 13. Figure 14 shows the radial force distribution when the rotor is out of the center by 0.1 mm, 0.25 mm, and 0.45 mm in the x-direction. From this figure, it is clear that the radial force is asymmetrical because the air gap field is unbalanced.

The resultant radial force is obtained by using the static solver when the rotor is located in the y-direction at 0.1 mm, 0.25 mm, and 0.45 mm, respectively, the resultant radial force over one rotor revolution is shown in Figure 15. The same behavior can be seen in figure 16 when the rotor moves toward the x-direction.

When the rotor is displaced towards angle 45° by 0.14142 mm, and then by 0.35355 mm, the resultant radial force over one rotor revolution is shown in Figure 17.

From Figures 12, 15, 16, and 17, it can be concluded that the resultant radial force is about zero when the rotor is at the center, while the radial force is unsymmetrical. The resultant have high values when the rotor is displaced. Asymmetry of radial force and resulting values increase with eccentricity.

Using a transient solver, the radial force produced by both the permanent magnet and the current stator winding can be evaluated. The waveform of the stator 3-phase current (112A) is shown in Figure 18. When the rotor rotates at the center (no eccentricity), the resultant radial force over one rotor revolution is shown in Figure19. Figure 20 shows the radial force

distribution when the rotor is out of the center by 0.1mm, 0.25mm, and 0.45mm in the x-direction, respectively. Figure 21 shows the radial force distribution when the rotor is out of the center by 0.1mm, 0.25mm, and 0.45mm in the y-direction, respectively. Figures 20 and 21 show that the radial force is still asymmetrical because of the unbalanced air gap field. The asymmetry is directly proportional to the rotor displacement from the center.

When the rotor is displaced toward x-direction by 0.1 mm, 0.25 mm, and 0.45 mm, the resultants are shown in Figure 22. When the rotor is replaced toward y-direction by 0.1 mm, 0.25 mm, and 0.45 mm, the resultants of radial force are shown in Figure 23.

When the rotor is displaced in both x and y direction and eccentricity toward 45° by 0.14142mm, and 0.35355mm, respectively, the resultants of radial force are shown in Figure 24.

All the results are tabulated in Table 2. For each of the cases, the table includes the minimum and maximum values of the radial force. Comparison between the results of the Magnetostatic analysis, which evaluates only the effect of the permanent magnet, and the transient analysis, which assesses the impact of both the permanent magnet and the armature current, the radial force is always greater in the transient analysis. In the study of variation of the radial force with the rotor position, it turns out that the radial force has a minimum value (about zero) at the center, and it increases as the rotor moves away from the center. The results obtained in this analysis introduce the next work, which minimizes or even cancels the radial force in the BLDC motor. This issue has great importance in bearingless motor design.

When the rotor is located at position (0, 0.1) mm and the armature winding current is 160 A and 209 A, respectively, the resultants of radial forces are as shown in Figure 25.

Table 2: Radial forces at the different rotor position

Rotor position (mm)	Radial force (N)		Transient analysis	
	Magnetostatic analysis Max. value	Min. value	Max. value	Min. value
At center (0,0)	14.8	0.2	13.304	0.9589
(0.1,0)	1335.8	1246.4	1348.488	915.191
(0.25,0)	3443.8	3177.4	3474.966	2325.606
(0.45,0)	6574.7	6021.8	6635.423	4368.688
(0,0.1)	1335.3	1246.7	1348.721	915.277
(0,0.25)	3443.8	3177.5	3474.022	2329.909
(0,0.45)	6574.9	6021.7	6634.322	4368.706
(0.14142, <45°)	2688.8	2578.2	2713.464	1230.162
(0.35355, <45°)	7220.2	7117.3	7192.185	4786.088

For these two cases, the results are tabulated in Table 3, and the radial force increases with the increase in armature current.

Table 3: Radial forces at different winging current

Rotor position (mm)	Armature current (A)	Radial force (N)	
		Max. value	Min. value
(0.1,0)	160	1205.387	447.983
(0.1,0)	209	1279.443	616.596

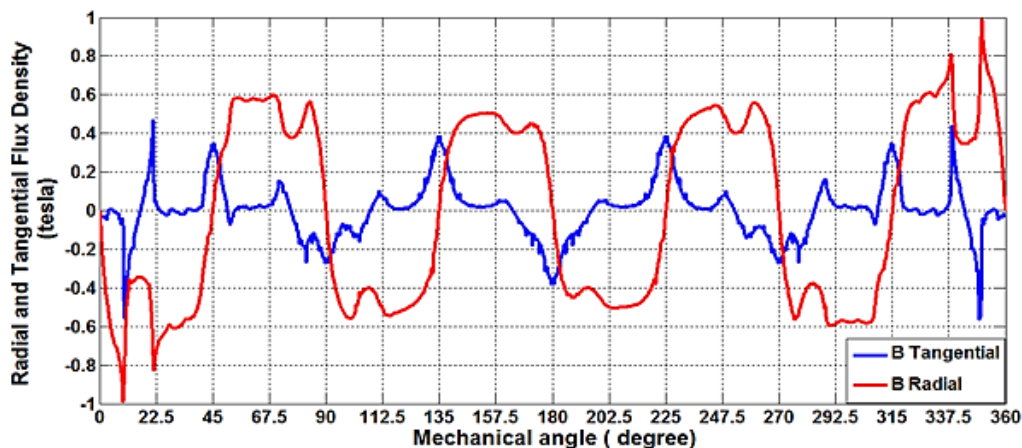


Figure 10: Radial and tangential flux density when the rotor moved by 0.45 mm in the x-axis direction

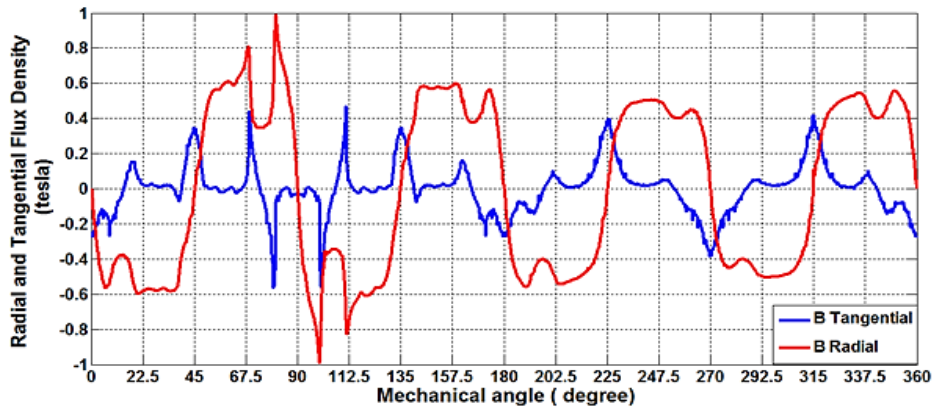


Figure 11: Radial and tangential flux density when the rotor moved by (0.45) mm in the y-axis direction

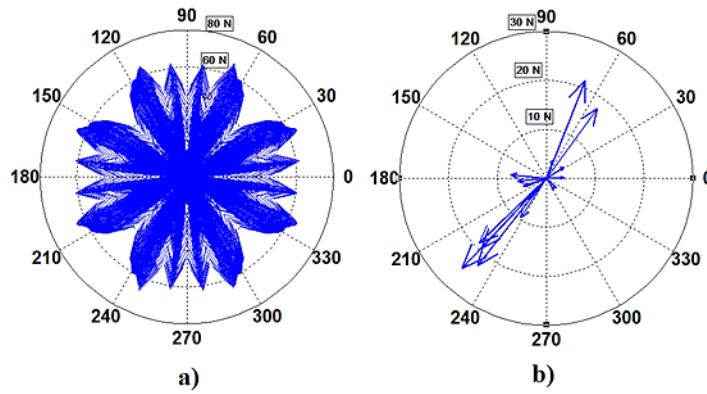


Figure 12: Radial force distribution (in N): (a) Instantaneous force, (b) Resultant force vectors

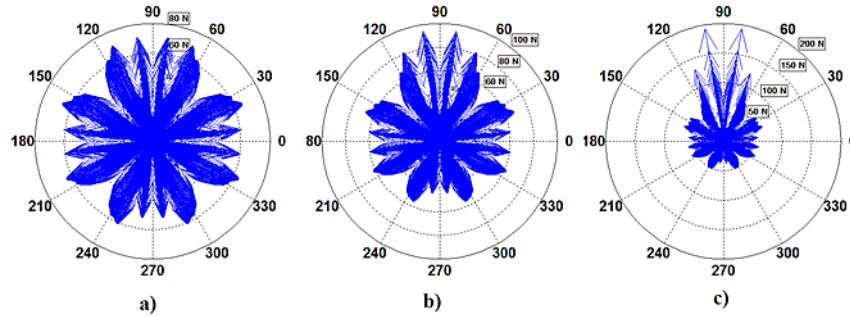


Figure 13: Radial force distribution when the rotor is displaced by:(a) 0.1mm, (b) 0.25mm, and (c) 0.45mm from the center in the y-direction

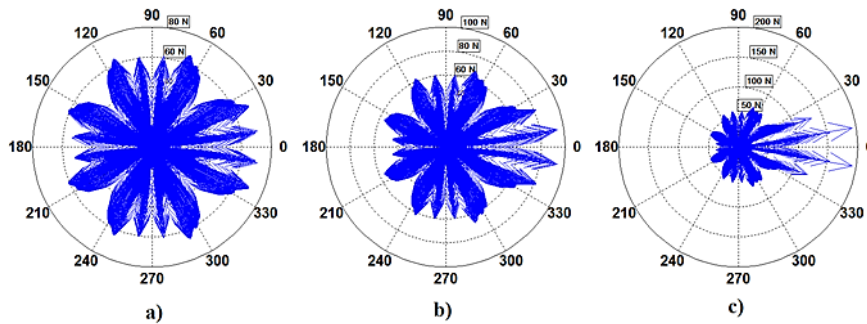


Figure 14: Radial force distribution when the rotor is displaced from the center in the x-axis by (a) 0.1mm, (b) 0.25mm, and (c) 0.45mm

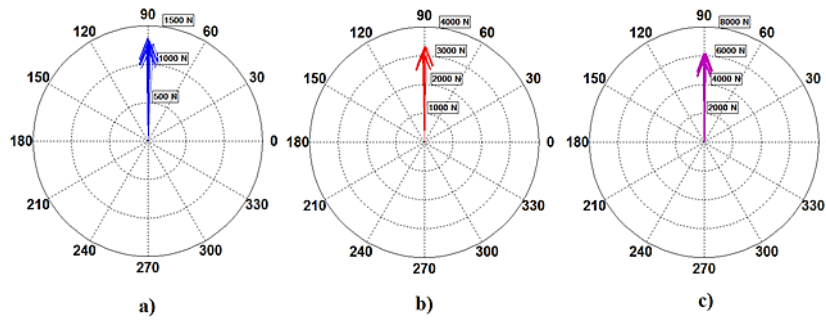


Figure 15: Resultant radial force when the rotor is displaced in the y-direction by: (a) 0.1mm, (b) 0.25mm, and (c) 0.45mm

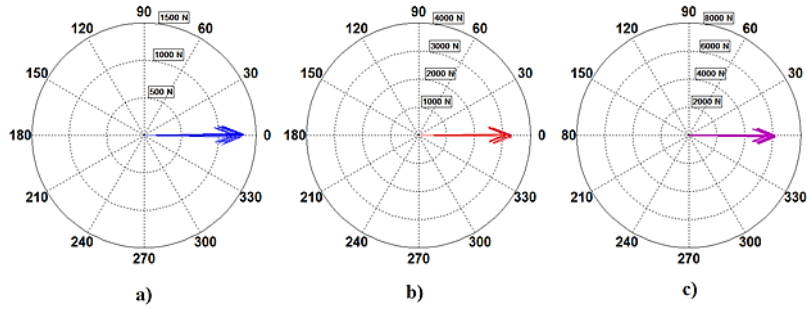


Figure 16: Resultant radial force when the rotor is displaced in the x-direction by: (a) 0.1mm, (b) 0.25 mm, and (c) 0.45 mm

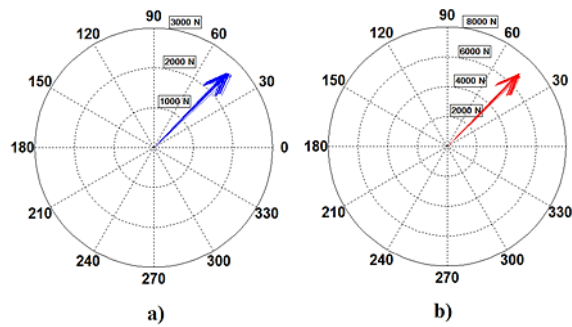


Figure 17: Resultant radial force when the rotor is displaced toward 45° direction by: 0.14142mm, and (b) 0.35355 mm

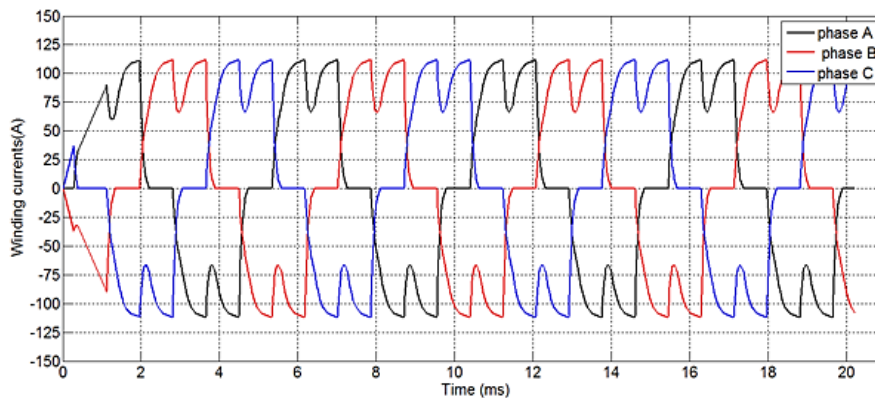


Figure 18: 3-phase stator current waveform

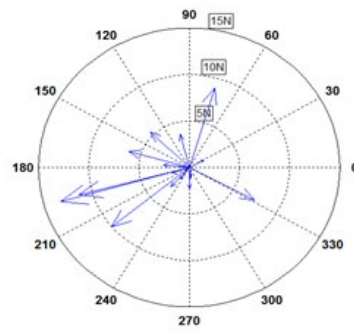


Figure 19: Resultant radial force vector when the rotor is at the center

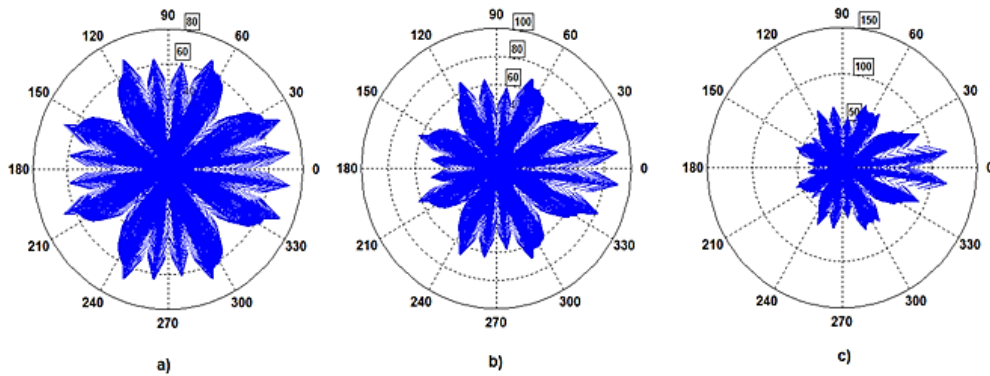


Figure 20: Radial force directions when the rotor is displaced in the x-direction by: (a) 0.1mm, (b) 0.25mm, and (c) 0.45mm

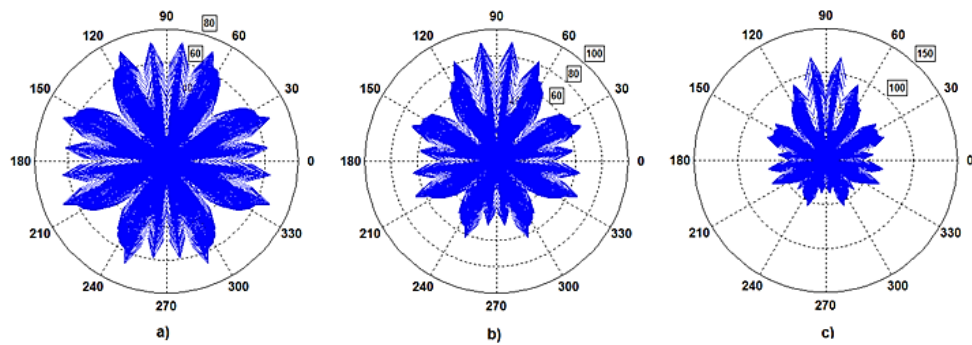


Figure 21: Radial force distribution when the rotor displaced in the y-direction by: (a) 0.1mm, (b) 0.25mm, and (c) 0.45mm

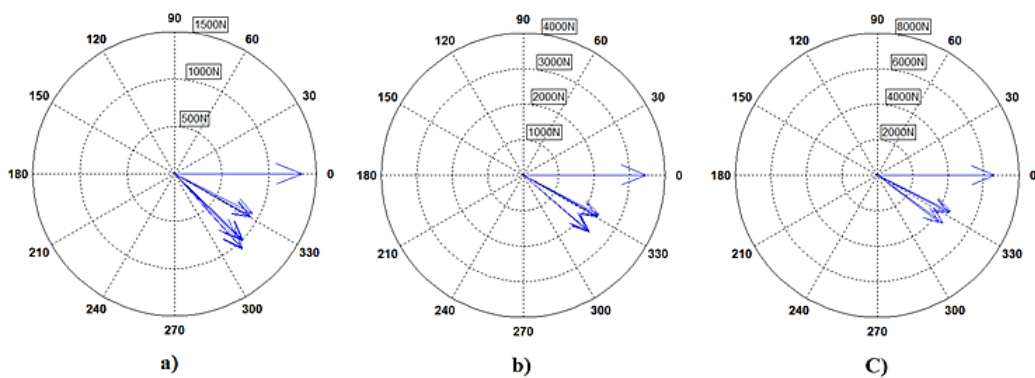


Figure 22: Resultant radial force directions when the rotor is displaced in the x-direction by: (a) 0.1mm, (b) 0.25mm, and (c) 0.45mm

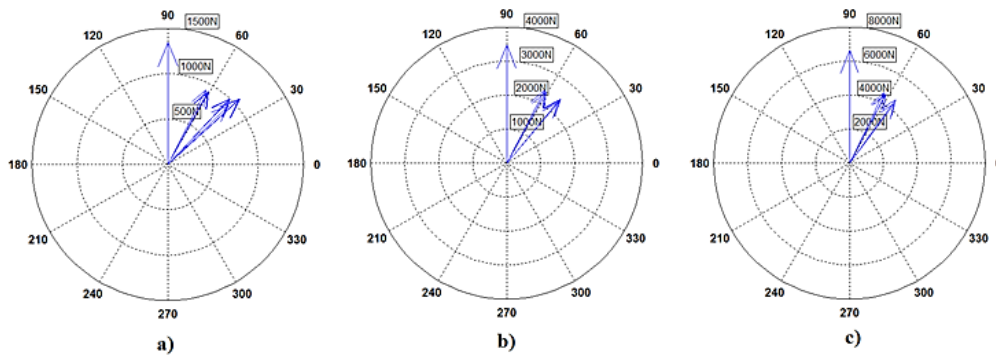


Figure 23: Resultant radial force when the rotor is displaced in the y-direction by: (a) 0.1mm, (b) 0.25mm, and (c) 0.45mm

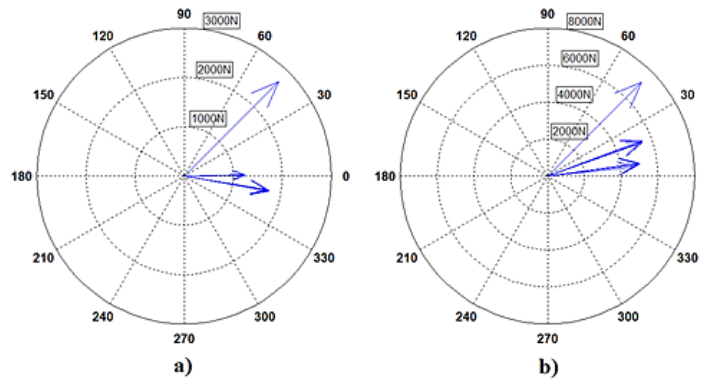


Figure 24: Resultant radial force when the rotor is displaced toward angle (45°) by (a) 0.14142 mm, and (b) 0.35355mm

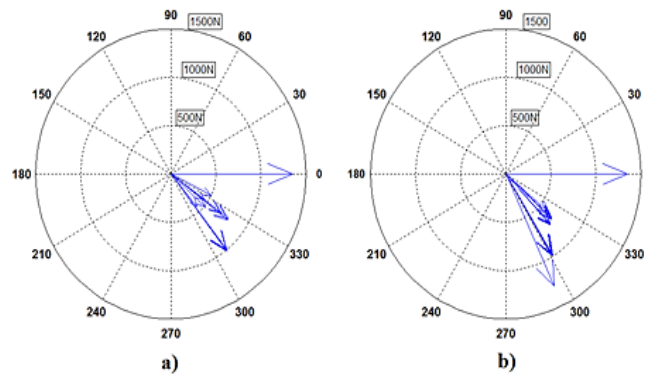


Figure 25: Resultant radial force when the rotor is moved by 0.1mm in the x-direction with the current of (a) 160 A, and (b) 209 A

5. Conclusions

The eccentricity of the rotor in electrical machines greatly influences the distribution of magnetic flux in the air gap and causes a high unbalance of radial forces and vibration. A numerical model has been developed in this paper to evaluate the forces based on finite element analysis. 12 slot/ 8 pole BLDC machine topology has been selected. This motor is used in a blood pump application. It can be seen that the lowest value of the radial forces exists when the rotor is at the center position. The radial force increases directly with the rotor displacement. It has been found that the radial forces at different rotor angles are also various because the reluctance of the air gap varies with rotating angle depending on pole pitch, stator teeth, and stator current direction. This study also showed increasing the stator current on the radial force. The proposed work can be considered the first step in bearing less motor design, and the obtained results can be used to design a control system for the bearing less BLDC motor.

Author contribution

All authors contributed equally to this work.

Funding

This research received no specific grant from any funding agency in the public, commercial, or not-for-profit sectors.

Data availability statement

The data that support the findings of this study are available on request from the corresponding author.

Conflicts of interest

The authors declare that there is no conflict of interest.

References

- [1] C. Xia, Mathematical Model and Characteristics Analysis of the BLDC Motor, Permanent Magnet Brushless DC Motor Drives and Cont., (2012) 25-62.
- [2] C.-I. Xia, Permanent magnet brushless DC motor drives and controls: John Wiley . Sons, (2012).
- [3] M. Ooshima , M. A. Rahman, Control strategy of magnetic suspension and performances of a bearingless BLDC motor, IEEE. Inte. Elec. Mac. Dri. Conf ., (2011) 71-76. <http://dx.doi.org/10.1109/IEMDC.2011.5994900>
- [4] Y. Qin , H. Zhu, Optimal design of a multi-phase double-stator bearingless brushless direct current motor, Adv. Mech. Eng., 9 (2017) 1687814017705112. <https://doi.org/10.1177/1687814017705112>
- [5] R. S. Raheem, Y. Y. Mohammed, S. K. Kadhim, Simulation Design of Blood-pump Intelligent Controller Based on PID - like fuzzy logic Technique, J. Eng. Technol., 38 (2020) 1200-1213. <https://doi.org/10.30684/etj.v38i8A.534>
- [6] N. W. Liu, K.Y. Hung, S. C. Yang, F. C. Lee, C. J. Liu, Design of High-Speed Permanent Magnet Motor Considering Rotor Radial Force and Motor Losses, Energies, 13 (2020) 5872. <https://doi.org/10.3390/en13225872>
- [7] X. Tu, W. Bu, Q. Zeng, Research on the Modelling of a Single-winding Bearingless Permanent Magnet Brushless DC Motor, J. Phys. Conf. Ser., 1887 (2021) 012049. <https://doi.org/10.1088/1742-6596/1887/1/012049>
- [8] A. Chiba, T. Fukao, O. Ichikawa, M. Oshima, M. Takemoto, D. G. Dorrell, Magnetic bearings and bearingless drives: Elsevier, (2005).
- [9] J. Pyrhonen, T. Jokinen, V. Hrabovcova, Design of rotating electrical machines, John. Wiley. Sons, (2013).
- [10] R. Islam , I. Husain, Analytical model for predicting noise and vibration in permanent-magnet synchronous motors, IEEE Trans. Ind. Appl., 46 (2010) 2346-2354. <https://doi.org/10.1109/TIA.2010.2070473>
- [11] W. Zhu, S. Pekarek, B. Fahimi, B. J. Deken, Investigation of force generation in a permanent magnet synchronous machine, IEEE. Trans. Ene. Conv., 22 (2007) 557-565. <https://doi.org/10.1109/TEC.2006.888034>
- [12] L. Zhou , D. L. Trumper, Reluctance force magnetic suspension characteristics and control for cylindrical rotor bearingless motors, J. Dyn. Sys. Meas. Control. Mar.,139 (2017) 031003. <https://doi.org/10.1115/1.4035007>
- [13] M. Y. Bdewi, A. M. Mohammed, M. M. Ezzaldean, Design and Performance Analysis of Permanent Magnet Synchronous Motor for Electric Vehicles Application, Eng. Tec. J., 39 (2021) 394-406. <https://doi.org/10.30684/etj.v39i3A.1765>
- [14] H. Dogan, F. Wurtz, A. Foggia, L. Garbuio, Analysis of slot-pole combination of fractional-slots pmsm for embedded applications, Int. Aeg. Conf. Elec. Mac. Power. Elec. Electr., (2011) 611-615. <https://doi.org/10.1109/ACEMP.2011.6490669>
- [15] F. Wang, Y. Zhu, H. Wang, D. Zhao, Design and analysis of a bearingless permanent-magnet motor for axial blood pump applications, IEEE Access, 8 (2019) 7622-7627. <https://doi.org/10.1109/ACCESS.2019.2959633>